CEAS-GNC-2024-026

EuroGNC Navigation Guidance Control CEAS Bristol, UK June 11th-13th 2024
University of BRISTOL ROYAL AERONAUTICAL SOCIETY AIAA

Asymmetric Cessna Citation II Stall Model Identification using a Roll Moment-based Kirchhoff Method

D. de Fuijk Master Student, Control and Simulation, TU-Delft, 2629HS, Delft, the Netherlands. d.defuijk@gmail.com

D.M. Pool Assistant Professor, Control and Simulation, TU-Delft, 2629HS, Delft, the Netherlands. d.m.pool@tudelft.nl

C.C. de Visser Associate Professor, Control and Simulation, TU-Delft, 2629HS, Delft, the Netherlands. c.c.devisser@tudelft.nl

ABSTRACT

Accurate modeling of the unsteady aerodynamics during flow separation is critical for effective pilot stall training in Flight Simulation Training Devices and the development of automatic stall recovery controllers. Kirchhoff's theory of flow separation has gained popularity due to its relative simplicity and suitability for parameter identification from flight data. The goal of this work is to improve an existing Cessna Citation II dynamic stall model's fidelity by applying Kirchhoff's method for each wing surface, separately. The main contribution is the identification of asymmetric flow separation development using the flight-derived roll moment and a roll moment model based on the differential flow separation between the wing surfaces. The longitudinal model structures are adopted from the existing, validated baseline stall model. The lateral-directional model outputs are in good agreement with the validation flight data, showing an average reduction of 48% in Mean Squared Error (MSE) compared to the baseline stall model. In contrast, the longitudinal model output results in an average MSE increase of 88%, suggesting that the estimated asymmetric flow separation parameters are unsuitable for longitudinal stall modeling. Hence, a hybrid approach is proposed that combines separate sets of flow separation parameters for the longitudinal and lateral-directional models.

Nomenclature

a	=	Linear acceleration [m/s^2]
$\mathbf{a}$	=	Regression variable vector
A	=	Regression matrix
a_1	=	Flow separation parameter - shaping [-]
b	=	Aircraft wing span [m]
$\bar{c}$	=	Mean chord length [m]
C_*	=	Aerodynamic force/moment coefficient [-]

I_* = Mass moment of inertia about *-axis [kgm^2]
J = Objective function value [-]
l = Aircraft length [m]
m = Aircraft mass [kg]
M = Mach number [-]
n = Load factor [-] (unless otherwise specified)
N = Number of data points
$\mathbf{p}$ = Orthogonalized regression variable vector
p, q, r = Pitch / roll / yaw rate [rad/s]
R^2 = Explained variance [-]
S = Wing surface aera [m^2]
X = Flow separation point variable [m]
y_w = Moment arm of single-wing lift vector [m]
α = Angle of attack [°]
α^* = Flow separation scheduling parameter [rad]
β = Sideslip angle [°]
ΔK_α = Kirchhoff regressors differential [-]
δ_a = Aileron deflection [°]
δ_e = Elevator deflection [°]
δ_r = Rudder deflection [°]
ϵ = Residual vector
$\gamma_{k,j}$ = Gram-Schmidt scaling parameter [-]
ϕ = Bank angle [°] / orthogonal parameter vector
ψ = Heading angle [°]
ρ = Pearson's linear correlation coefficient [-]
σ = Standard deviation
σ_y = Scaling parameter for PSE metric [-]
τ_1 = Flow separation parameter, transient effects [s]
τ_2 = Flow separation parameter, quasi-steady effects [s]
θ = Pitch angle [°] / parameter vector

Subscripts

0 = Steady state / Initial value
b = Body-fixed reference frame
D = Drag force
l = Roll moment
L = Lift force / Left wing
m = Pitch moment
n = Yaw moment
R = Right wing
T = Thrust force
Y = Lateral force

Superscripts

$\bar{}$ = Mean value
$\dot{}$ = Time-derivative
$\hat{}$ = Estimate
$^\top$ = Transpose vector

1 Introduction

Aerodynamic forces and moment models are traditionally based on stability and control derivatives [1]. This approach has led to adequate dynamic aircraft models for the nominal flight envelope. However, in stall and post-stall flight conditions, aerodynamic forces and moments exhibit nonlinear and noticeable unsteady effects as a result of flow separation. Furthermore, the effectiveness of a control surface can be reduced due to potential interactions with the turbulent wake resulting from separated flow. A

recent study conducted wind tunnel experiments with a scaled aircraft model to investigate lateral control authority during stall, identifying a reduction of approximately 40% in aileron effectiveness [2]. Adequate modeling of such unsteady aerodynamics during flow separation is critical for pilot training in Flight Simulation Training Devices (FSTDs), for upset situations and loss-of-control in flight (LOC-I) [3, 4], as nearly 40% of LOC-I accidents are categorized as stall-related [5].

Recently, Computational Fluid Dynamics (CFD) methods have been employed to evaluate complete aircraft stall models [6]. The EU-funded project "Simulation of Upset Recovery in Aviation" (SUPRA) introduced a complex approach, based on wind tunnel data and complemented by CFD analysis [4, 7]. While these methods can achieve high levels of accuracy, they often come with the drawbacks of being computationally expensive and requiring rigorous validation procedures. Hence, model identification from flight data remains relevant.

A popular stall modeling approach is based on Kirchhoff's theory of flow separation. First introduced by [8], Kirchhoff's method aims to model the lift using an internal flow separation variable X, a coordinate describing the location of the flow separation point on the upper airfoil surface. Conveniently, this variable has also been shown to adequately model nonlinear effects that occur in the drag and the pitch moment coefficients [9, 10]. A direct measurement of the flow separation point is difficult to obtain. Alternatively, it has been approximated using a first-order ordinary differential equation (ODE), of which the parameters are estimated from wind tunnel tests, flight data, or a combination of the two [9–11]. The main limitation of Kirchhoff's method is that the flow separation point is generally considered as a one-dimensional coordinate, rendering it unsuitable for describing any flow separation asymmetry. To combat this issue, [12] modeled the normal force on each wing separately using Kirchhoff's theory, whereas [13] included additional lift surfaces and applied a quadratic polynomial approximation. This paper explores variants of the first two approaches. Alternatively, in [14] a geometric (wing) segmentation approach was introduced to model asymmetric stall.

The goal of this work is to improve a previously developed Cessna Citation II dynamic stall model's fidelity [15] by applying asymmetric stall modifications to Kirchhoff's method. The main contribution is the identification of asymmetric flow separation development, using the flight-derived roll moment and a roll moment model that explicitly accounts for the differential flow separation between the wing surfaces. Additionally, an attempt is made to identify any variations in lateral-directional control effectiveness. To reach the set objectives, flight experiments were conducted using TU Delft's laboratory aircraft, dedicated to gathering data containing strong asymmetric and dynamic excitation, as well as control surface deflections, during accelerated stall maneuvers. The flow separation parameters are identified through a nonlinear optimization, and the resulting separation variables are subsequently treated as fixed internal state variables. For this purpose, a roll-moment model structure is selected based on an analysis of Kirchhoff's model and an alternative first-order approximation.

The performed flight experiments and the resulting data are detailed in Section 2. Subsequently, the system identification methodology is explained in Section 3. Section 4 presents the results of the model identification and validation processes. The main conclusions are summarized in Section 6.

2 Flight Experiments and Data

2.1 Research Aircraft

All flight experiments were conducted with a Cessna Citation II (550) aircraft (PH-LAB), a twin-jet originally built for executive travel. The PH-LAB is co-owned by TU Delft and Netherlands Aerospace Center (NLR). A custom Flight Test Instrumentation System (FTIS) is installed, which aggregates all the measurement data from the sensors. For this research, a crucial part of the measurement equipment is the air data boom connected to the aircraft nose, as highlighted along with the body-fixed reference frame

in Fig. 1. This device allows for accurate measurements of the airflow angles. Important geometry and mass/inertia properties of the aircraft are given in Table 1.

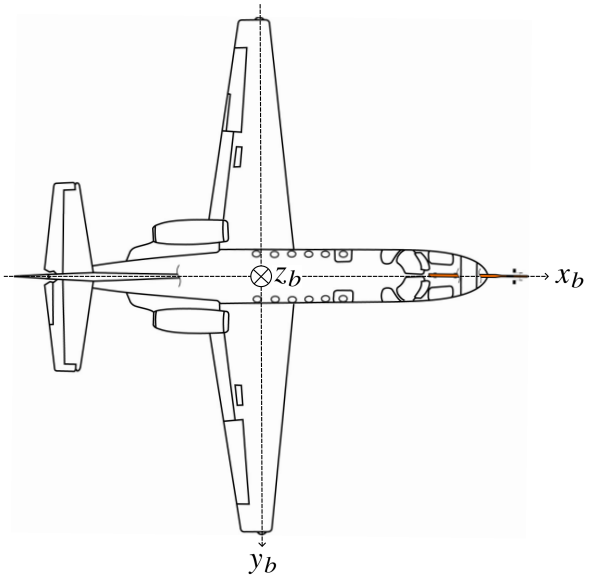

Fig. 1 Top view of the research aircraft, including the body-fixed reference frame and a highlighted air data boom. Adapted from [15].

Table 1 Cessna Citation II general specifications (BEW=Basic Empty Weight).

Dimensions			**Mass and inertia (BEW)**		
b	15.9	m	MTOW	6600	kg
l	14.4	m	MLW	6100	kg
$\bar{c}$	2.09	m	BEW	3900	kg
S	30.0	m^2	I_{xx}	12392	kgm^2
			I_{yy}	31501	kgm^2
			I_{zz}	41908	kgm^2
			I_{xz}	2252.2	kgm^2

2.2 Experiment Design

All new stall maneuvers were conducted in clean configuration, between Flight Level (FL) 150 and 200. Since a large bulk of the previous stall data was gathered at this altitude [15], this choice allows for model validation using a combination of the data sets.

The classic quasi-steady stall maneuver, during which the airspeed is reduced at approximately -1 kt/s, has proven ineffective for parameter estimation purposes [10]. In this condition, unsteady state variables such as pitch rate q and angle of attack rate $\dot{\alpha}$ are close to zero, while other states vary simultaneously and approximately linearly, leading to strong correlations. These conditions make parameter estimation a difficult task and any resulting model will be of a low fidelity. Instead, two types of dynamic maneuvers were applied during the stall maneuvers, quasi-random disturbance (QR) inputs and 3-2-1-1 inputs. Both input types are displayed in Fig. 2. QR refers to the pilot attempting to apply quasi-random inputs with as little correlation as possible, a piloting technique based on the description of [16] with the goal of obtaining excitation for a large input bandwidth. During the experiments, a fly-by-wire system was available to apply automatic 3-2-1-1 inputs, ensuring reliable dynamic roll axis excitation [17]. To avoid reaching excessively large bank angles (which could lead the aircraft into a spin), it was chosen to direct the longest positive input (”3”) in the opposite direction of the stall approach bank angle, with an amplitude scaled such that no excessive bank angles where achieved on the second ("2") pulse in the direction of the stall approach bank angle. Hence, all 3-2-1-1 maneuvers were initiated to the left.

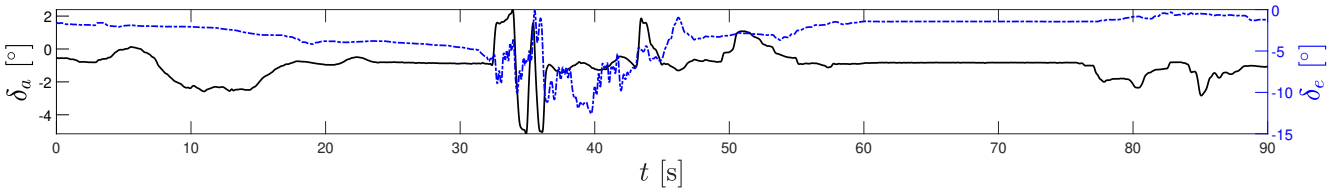

Fig. 2 An example of a simultaneous 3-2-1-1 aileron input and a QR elevator input.

The newly conducted experiments are exclusively $1.1g$ accelerated stalls (to the right), with the purpose of inducing asymmetric flow separation effects. The term "accelerated" refers to a stall maneuver that is performed with a reference bank angle, or load factor n_z. To further impose asymmetry, 6 stall maneuvers were performed with a reference sideslip angle. The objective was to reach $\beta_{\text{ref}} = 5°$, which was in practice difficult to maintain for the pilots. The fact that this choice required significant rudder inputs provided an additional benefit for parameter identification, as [15] noted that only a subset of the previous data included sufficient rudder inputs for accurate estimation of the yaw moment model parameters.

3 Modeling and System Identification Methodology

3.1 Kirchhoff's Flow Separation Model

The description of nonlinear behavior in the proposed stall model is based on Kirchhoff's theory of flow separation. In its original form, this model describes the lift coefficient of an airfoil C_L at high angle of attack α:

$$C_L = C_{L_\alpha} \left(\frac{1 + \sqrt{X}}{2} \right)^2 \alpha \tag{1}$$

where C_{L_α} is the airfoil's lift slope. The flow separation point X is a non-dimensional coordinate that represents the position of the separation point on the upper surface of the airfoil. It ranges from 0 to 1, where $X = 1$ indicates fully attached flow and $X = 0$ corresponds to fully separated flow [8]. According to Kirchhoff's theory, X is the solution to the following ODE:

$$\tau_1 \frac{dX}{dt} + X = \frac{1}{2} \left\{ 1 - \tanh \left(a_1 \left(\alpha - \tau_2 \dot{\alpha} - \alpha^* \right) \right) \right\}, \tag{2}$$

with a_1 a shaping parameter that describes the abruptness of the stall, α^* the stall angle of attack, τ_1 models transient effects, while τ_2 captures hysteresis from attached flow to flow separation, and vice versa.

3.2 Asymmetric Stall Modeling using the Roll Moment

The aerodynamic coefficient that is most important for describing asymmetric stall characteristics is the roll moment coefficient, as it is directly dependent on lift differentials between the lifting surfaces (e.g., wing, tail) on both sides of the aircraft. In this research, only the differential between the main wing surfaces is considered. The individual surface lift coefficients are modeled by Kirchhoff's model.

$$\Delta \hat{C}_l = \left[(C_{L_\alpha})_L \left(\frac{1 + \sqrt{X_L}}{2} \right)^2 \alpha_L - (C_{L_\alpha})_R \left(\frac{1 + \sqrt{X_R}}{2} \right)^2 \alpha_R \right] \frac{y_w}{b} \tag{3}$$

where X_L and X_R are the flow separation variables for the left and right wing, and α_L and α_R the local angle of attack at a distance y_w on the left and right wing surface, respectively.

Symmetric wings would imply equal airfoil properties, resulting in the simplification $C_{l_{\Delta K_\alpha}} = (C_{L_\alpha})_L = (C_{L_\alpha})_R$. For simplicity, the notation ΔK_α is introduced:

$$\Delta \hat{C}_l = C_{l_{\Delta K_\alpha}} \Delta K_\alpha \frac{y_w}{b} \quad \text{with} \quad \Delta K_\alpha = \left(\frac{1 + \sqrt{X_L}}{2} \right)^2 \alpha_L - \left(\frac{1 + \sqrt{X_R}}{2} \right)^2 \alpha_R \tag{4}$$

Note that Kirchhoff's model was developed for complete airfoils, not single (half) wings. In Eq. 4, it is assumed that it can provide an adequate description of the difference in lift between individual wing surfaces. Considering the fact that Kirchhoff's model may not be suitable for a single wing surface, a simpler alternative description of asymmetric stall is proposed:

$$\Delta\hat{C}_l = C_{l_{\Delta X}} \Delta X \frac{y_w}{b} \quad \text{with} \quad \Delta X = (X_L - X_R) \tag{5}$$

Eq. 5 is a simplification of Lutze et al.'s model [13]: the dependence of the left wing surface lift on X_L, is approximated as a first-order polynomial, where the bias is included in the general bias term of the model (C_{l_0}). The same holds for the right wing surface. The symmetry property of the aircraft is again taken into account, to obtain a single parameter $C_{l_{\Delta X}}$. The flow separation variables are each governed by their own ODEs:

$$(\tau_1)_{L,R} \frac{dX_{L,R}}{dt} + X_{L,R} = \frac{1}{2}\left\{1 - \tanh\left(a_1\left(\alpha_{L,R} - \tau_2 \dot{\alpha}_{L,R} - \alpha^*\right)\right)\right\} \tag{6}$$

Finally, for the longitudinal models, the symmetric flow separation variable X is computed by taking the mean of X_L and X_R at every data point:

$$X = \frac{X_L + X_R}{2} \tag{7}$$

3.3 Local Angle of Attack Computation

The local angle of attack at an arbitrary point P is computed through a kinematic relationship that describes the local airflow velocity, whereby the aircraft is assumed to be a rigid body [18]:

$$\alpha_P = \text{atan}\left(\frac{w_P}{u_P}\right) = \text{atan}\left(\frac{w - q\Delta x_P + p\Delta y_P}{u - r\Delta y_P + q\Delta z_P}\right) \tag{8}$$

where $\Delta \boldsymbol{X_p} = [\Delta x_P \ \Delta y_P \ \Delta z_P]^\top$ are the distances from the aircraft center of gravity (CG) to the point P. For the left and right wings only the lateral offset is relevant: $\Delta \boldsymbol{X_{L,R}} = [0, \pm y_w, 0]^\top$. Since y_w is to describe a moment arm of the lift vector, ideally this value is equal to the distance to the center of lift of a single wing surface, measured from the fuselage center line. As an approximation, it is set equal to the lateral location of the Mean Aerodynamic Chord (MAC). Fig. 3 presents a reconstructed response of the local angles of attack to a 3-2-1-1 aileron input, during an accelerated stall maneuver. Note that the angle of attack at the CG (α) is assumed to be the mean of the local variants ($\alpha_{L,R}$), which may not be correct for large side-slip angles.

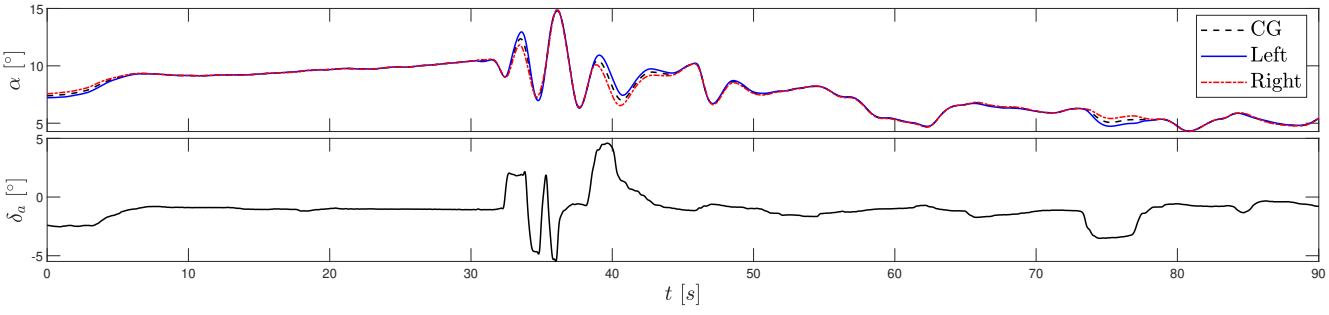

Fig. 3 The response of the local and general angle of attack to a 3-2-1-1 aileron input ($t \approx 30$ s to $t \approx 40$ s), during an accelerated stall maneuver (ASYM set 21).

3.4 Identification Problem and Approach

The main objective of the identification procedure is the creation of a 6-DOF aerodynamic model of the aerodynamic force and moment coefficients. As such, the downstream identification task is the estimation of the parameter vectors (θ) of the coefficients of lift (C_L), drag (C_D), lateral force (C_Y), roll moment (C_l), pitch moment (C_m), and yaw moment (C_n):

$$\hat{\theta}_{C_L}, \hat{\theta}_{C_D}, \hat{\theta}_{C_Y}, \hat{\theta}_{C_l}, \hat{\theta}_{C_m}, \hat{\theta}_{C_n} \tag{9}$$

The X-parameters provide a convenient description of the flow separation variables. Once these parameters are known or estimated, X_L and X_R can be determined by solving their respective ODEs, i.e. Eq. (6). Hence, the second set of parameters to estimate consists of the X-parameters:

$$\hat{\theta}_X = \begin{bmatrix} \tau_1 & \tau_2 & a_1 & \alpha^* \end{bmatrix}^\top \tag{10}$$

As previously proposed in [15], the parameter estimation approach is split into two parts: the nonlinear X-parameter estimation and the linear C_i-parameter estimation, see Fig. 4.

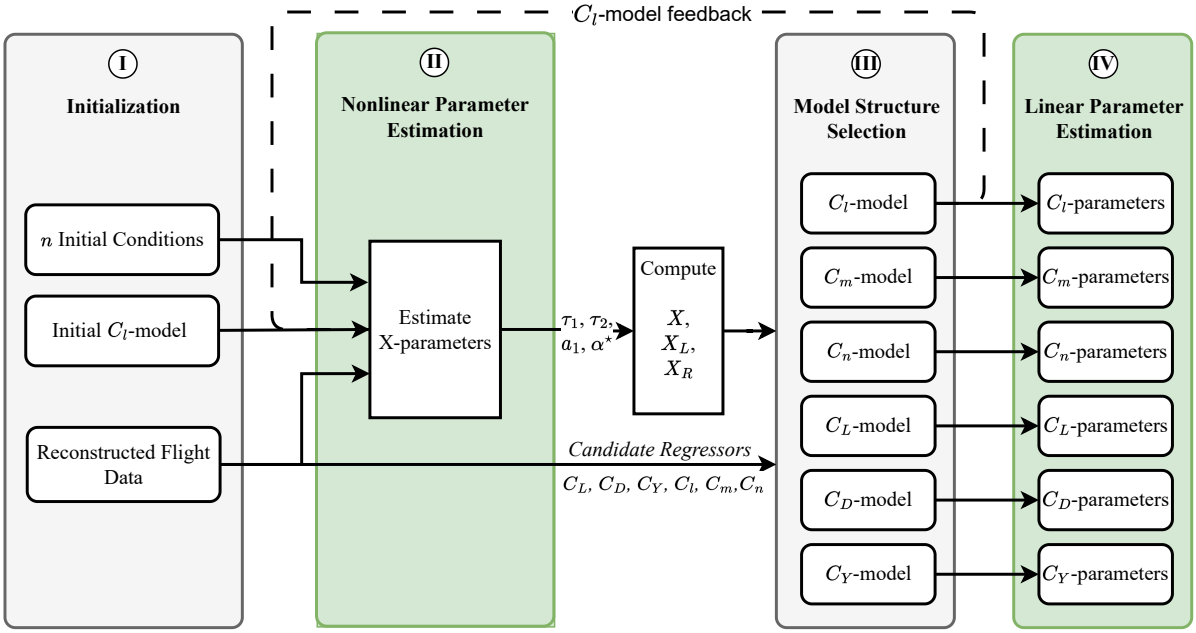

Fig. 4 A flowchart describing the proposed identification approach.

3.4.1 Step I: Initial Roll Moment Model Selection

To initialize the nonlinear optimization, an initial guess of a roll moment model structure is required. Note that this model structure is modified iteratively in Step II and Step III, see Fig. 4. The following conventional linearized model structure is suitable outside the stall region [19] and was used during initialization:

$$\hat{C}_l(x, \theta)_{\text{lin}} = C_{l_0} + C_{l_\beta}\beta + C_{l_p}p + C_{l_r}r + C_{l_{\delta_a}}\delta_a + C_{l_{\delta_r}}\delta_r \tag{11}$$

In order to identify asymmetric flow separation characteristics in Step II of Fig. 4, terms related to X_L and X_R must be included in the initial roll moment model. Two mathematical formulations of asymmetric stall were introduced in Section 3.2. The effectiveness of the parameter identification task is evaluated for both formulations, to determine whether a modification of Kirchhoff's model is required or

a simpler approximation is sufficient. Eq. (4) and Eq. (5) are appended to the conventional roll moment model to obtain the initial roll moment model for the structure selection process. In this paper, this model is referred to as Model B-I, where the "I" denotes that this is the first iteration of Model B.

$$\text{Model B-I} \quad \hat{C}_l(x,\theta)_0 = \hat{C}_l(x,\theta)_{\text{lin}} + C_{l_{\Delta X}} \Delta X \frac{y_w}{b} \quad \text{with} \quad \Delta X = (X_L - X_R) \tag{12}$$

Note that the simplicity of the additional term of model B comes from the exclusion of local angles of attack: once the X-parameters are estimated, these local computations are no longer required for evaluating the model output.

3.4.2 Step II: Nonlinear Parameter Estimation

A nonlinear optimization method is employed for the identification of the flow separation parameters. The nonlinearity of the problem originates from the ODEs of Eq. (6). The objective function is the mean squared error (MSE) of the roll moment model output $\hat{C}_l(\theta, x)$ with respect to the measured C_l:

$$\hat{\theta} = \arg\min_{\theta} J(\theta, x) \quad \text{with} \quad J(\theta, x) = \frac{1}{N} \left(C_l - \hat{C}_l(\theta, x) \right)^\top \left(C_l - \hat{C}_l(\theta, x) \right) \tag{13}$$

where $C_l, \hat{C}_l \in \mathbb{R}^{N \times 1}$ and N denotes the number of data points in a training set.

As mentioned in Section 3.1, the X-parameters are mostly dependent on airfoil and wing configuration. Only τ_1 is determined by the free-stream velocity. Both conditions are assumed to be equal between the wing surfaces. Hence, a single set of X-parameters is to be estimated:

$$(\theta_X)_L = (\theta_X)_R = \theta_X = \begin{bmatrix} \tau_1 & \tau_2 & a_1 & \alpha^* \end{bmatrix}^\top \tag{14}$$

The parameter vector associated with this optimization is the result of appending the C_l-parameters to the X-parameters. Note that these C_l-parameter estimates are not directly used for the final roll moment model. These additional estimates provide a method of verification of the optimization, as they should converge to similar values. For the first iteration, the introduced initial roll moment model structures yield the parameter vectors of the associated optimization problems:

$$(\theta_{nl})_B = \begin{bmatrix} \tau_1 & \tau_2 & a_1 & \alpha^* & C_{l_0} & C_{l_\beta} & C_{l_p} & C_{l_r} & C_{l_{\delta_a}} & C_{l_{\delta_r}} & C_{l_{\Delta X}} \end{bmatrix}^\top \tag{15}$$

Upper and lower bounds are enforced on the parameters, to shrink the solution space. The optimization is performed by an Interior Point algorithm implementation, using the `fmincon` function from MATLAB's optimization toolbox.

3.4.3 Step III: Model Structure Selection

The general objective of the model structure selection procedure (Step III in Fig. 4) is to generate a compact (parsimonious) model that retains adequate complexity to capture the nonlinearities associated with aircraft stall [20]. Minimizing the number of model terms enhances parameter identifiability, leading to improved accuracy in parameter estimates and prediction (validation) performance. The interdependence of the model structure selection tasks is further detailed in Fig. 5. The roll moment model structure $\hat{C}_l(x, \theta)$ must be selected first, as any changes in this model could result in different X-parameter estimates. Once these parameter estimates are fixed, the remaining model structures can be selected. Finally, it is chosen to keep the longitudinal model structures equal to those of the previous stall model, as these were shown to capture the nonlinearities of aircraft stall adequately [15]. The newly

estimated X-parameters are used for the evaluation of this model, providing the opportunity to evaluate the proposed method for the application of longitudinal modeling.

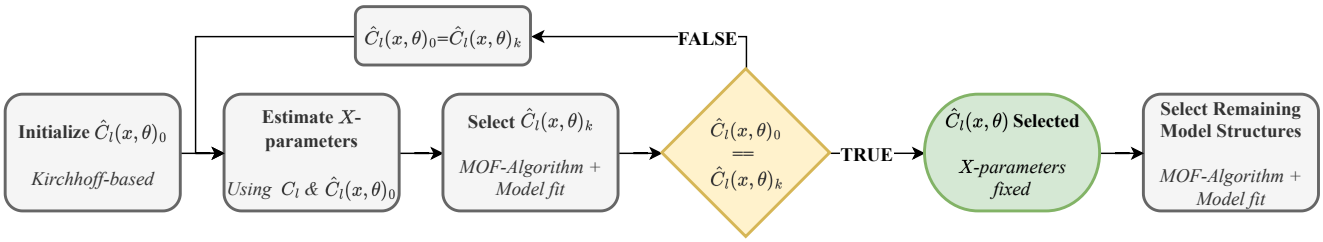

Fig. 5 The process of model structure selection using multivariate orthogonal functions (MOF), starting from the initial roll moment model.

Model structure selection and parameter estimation are coupled procedures. While selecting a model structure is a prerequisite for parameter estimation, evaluating the adequacy of a postulated model requires parameter estimates. This circular dependence makes the problem difficult to solve objectively [20]. A possible solution is the concept of stepwise regression, where statistical hypothesis testing is employed to select model terms from a pool of proposed terms [21]. An additional challenge lies in the potential correlation between independent variables. To tackle these challenges, [20] applied a Multivariate Orthogonal Functions (MOF) modeling algorithm, with the purpose of global aerodynamic modeling. Subsequent work has proven the effectiveness of this technique for the application of aircraft stall modeling [15, 16]. Hence, the MOF selection method is also employed in this paper.

The reconstructed flight data amounts to a pool of candidate regressors, to be used in the model structure selection. The performance of the described selection algorithm relies completely on the combined explanatory value of this candidate pool. The pool of candidate regressors considered in this paper can be found in Table 2. Several different categories of regressors are identified. A bias term is included in every model. To employ additional a priori knowledge, a linearized quasi-steady analytical aircraft model is taken as a reference [19], where a distinction is made between regressors that describe symmetric and asymmetric motion.

Table 2 The candidate regression variables categorized by model type.

Regressor Type	Symmetric	Asymmetric
Bias	**1**	**1**
Measured	$\alpha, q, C_T, M, \delta_e$	$\beta, p, r, \delta_a, \delta_r$
Time-derivative	$\dot{\alpha}$	$\dot{\beta}$
Flow Separation	$X, (1-X)$	$\Delta X \frac{y_w}{b}, \Delta K_\alpha \frac{y_w}{b}$

3.4.4 Step IV: Linear Parameter Estimation

Given a set of six linear-in-the-parameters model structures, Step IV concerns the identification of the C_i-parameters. The selected model structures are linear polynomials:

$$\hat{C}_i = \theta_{C_{i_1}} \boldsymbol{a}_1 + \theta_{C_{i_2}} \boldsymbol{a}_2 + \ldots + \theta_{C_{i_n}} \boldsymbol{a}_n, \quad \text{for} \quad i \in \{L, D, Y, l, m, n\} \tag{16}$$

where $\hat{C}_i$ is the model output of force or moment i, $\boldsymbol{a}_j$ are the regressor vectors and $\theta_{C_{i_j}}$ are the parameters from the vector θ_{C_i}. Using the matrix notation the equation reduces to the regression form:

$$\hat{C}_i = A\theta_{C_i}, \quad \text{with} \quad A = [\boldsymbol{a}_1\ \boldsymbol{a}_2\ \ldots\ \boldsymbol{a}_n] \tag{17}$$

An OLS solution is applied to minimize the model error $\epsilon = C_i - \hat{C}_i$, where C_i denotes the measurement vector. This results in the closed-form solution for all parameter vectors:

$$\hat{\theta}_{C_i} = (A^\top A)^{-1} A^\top C_i, \quad \text{for} \quad i \in \{L, D, Y, l, m, n\} \tag{18}$$

4 Results

The described methodology is applied to the flight test data to obtain the stall model. Due to the interdependencies in the approach of Fig 4, the order of presentation of the results is important. The initial roll moment model structure selection (Step I) was detailed in Section 3.4.1. Converging to a final roll moment model structure is a prerequisite for estimating the final set of X-parameters. Therefore, this process is described first (Step IIIa). Subsequently, the final nonlinear optimization results are detailed (Step II) and the remaining model structures are selected (Step IIIb). When the X-parameters and all model structures are fixed, the results of the linear regression step are shown (Step IV), presenting the complete stall model. Finally, the model is validated using a subset of the flight test data set.

4.1 Step IIIa: C_l-Model

The initial (Model B-I) and final (Model B) nonlinear optimizations of the X-parameters using the C_l measurement data results are presented in Table 3.

Table 3 X-parameter estimates of the initial (Model B-I) and final (Model B) roll moment models, for the C_l-model structure selection. Results are compared to the baseline model from [15]. The lowest standard deviation of a given parameter is bold-faced.

	Optimization	**Model B-I**		**Model B**		**Baseline Model [15]**	
θ	**Bounds**	$\hat{\theta}$	$\sigma_{\hat{\theta}}$	$\hat{\theta}$	$\sigma_{\hat{\theta}}$	$\hat{\theta}$	$\sigma_{\hat{\theta}}$
τ_1 [s]	[0.001, 0.50]	0.1166	0.0598	0.0971	**0.0282**	0.2547	0.1565
τ_2 [s]	[0.000, 0.80]	0.5386	0.1486	0.5526	0.1636	0.0176	**0.0819**
a_1 [-]	[15.00, 40.0]	17.269	2.9987	16.865	**1.1672**	27.671	6.7177
α^* [rad]	[0.100, 0.35]	0.1744	0.0363	0.1730	**0.0194**	0.2084	0.0202

In Fig. 6a the model structure for C_l resulting from the MOF algorithm are shown for the first and second MOF iterations, respectively. In the figures, the candidate regressors on the vertical axis are selected in the number of stall maneuvers as shown on the horizontal axis. A grey bar indicates that the corresponding regressor is frozen into the model, either due to selection in a previous iteration, or because it concerns a bias term. The iterations were terminated after the second iteration because no further significant improvements of the model fit were obtained after this.

The final structure of Model B is:

$$\hat{C}_l(x, \theta) = C_{l_0} + C_{l_\beta}\beta + C_{l_r} r + C_{l_{\delta_a}}\delta_a + C_{l_{\Delta X}}\Delta X \frac{y_w}{b} \tag{19}$$

It should be noted that the model structure in Eq. 19 does not contain a roll damping term (C_{l_p}), which was consistently rejected during the stepwise regression procedure due to lack of significance. Instead the effects of roll damping are captured in the $C_{l_{\Delta X}}\Delta X$ term. While this does lead to better

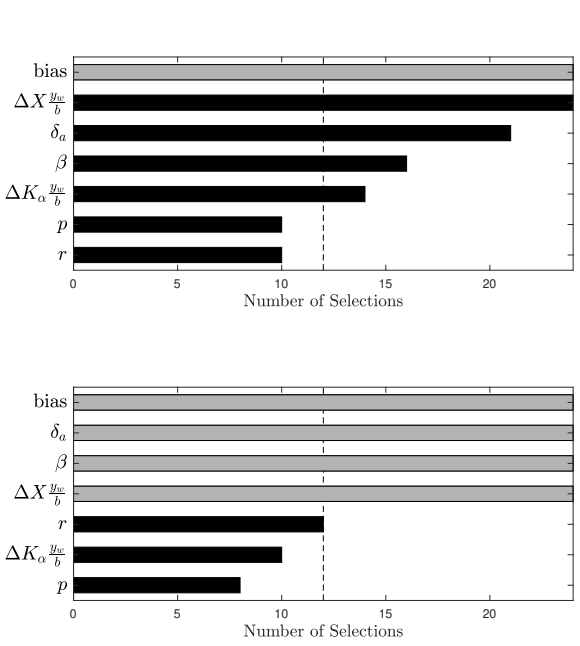

(a) Results of the first (top) and second (bottom) iterations of the MOF algorithm using C_l data. Grey bars indicate terms in the model structure that were fixed because of selection in a previous iteration, or because the considered term is a bias term which by default is always included. Horizontal axis counts the number of maneuver sets out of a total of 24, with dashed line indicating the 50% mark.

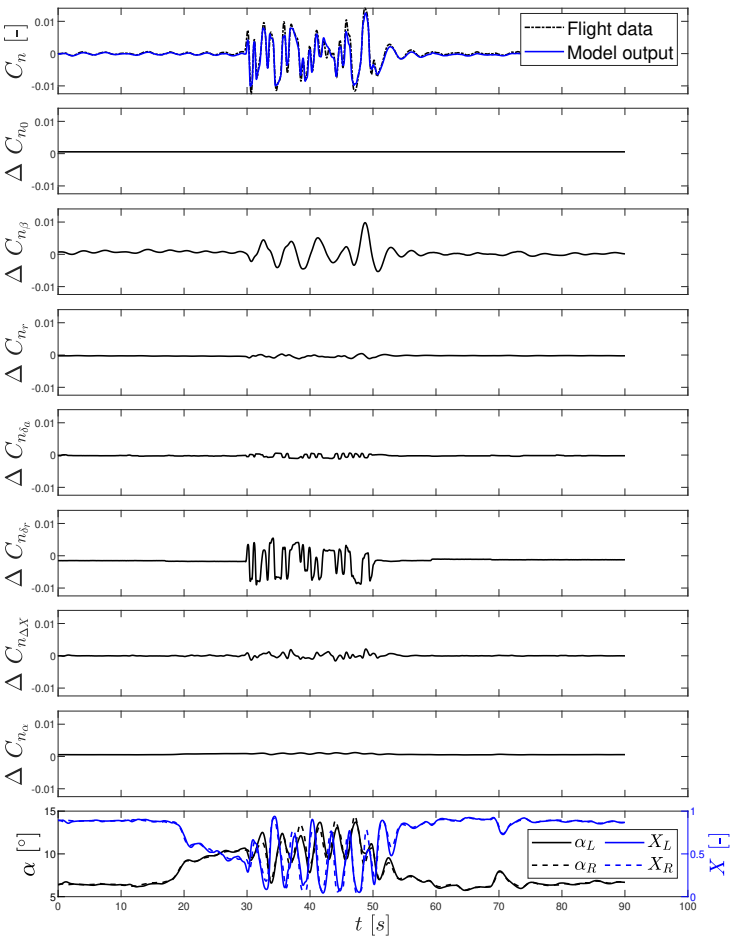

(b) Model term contributions, after OLS (ASYM set 7).

Fig. 6 Cl-Model structure selection algorithm results and final model term contributions

validation performance, this does lead to issues when blending the nominal (non-stall) aerodynamic model with the stall model.

Table 4 presents the model fit for the intermediate and final models, on the validation set. The model fit metrics that are used in this paper are MSE and the explained variance R^2.

Table 4 Performance of the intermediate and the selected model structures, evaluated by the validation fit.

Model Structure	MSE	$\bar{R}^2$	$min(R^2)$	$max(R^2)$
Model B-I	1.49E-6	0.74	0.55	0.85
Final Model B	1.41E-6	0.75	0.63	0.86

4.2 Step II: Nonlinear Optimization

The objective of Step II of Fig. 4 is to provide adequate estimates of the X-parameters. Since there is no flow separation measurement available, the estimates are analyzed by their variances, distributions, and a comparison with the baseline stall model. The optimization is verified by a cost function analysis and a comparison of nonlinear optimization results with the results of linear regression.

In the following discussions, only the final selected structure of Model B is considered. The X-parameter estimates and their standard deviations can be found in Table 3, for the proposed model and the baseline model [15].

4.3 Step IIIb: Remaining Force and Moment Coefficient Models

The remaining model structures are selected using the X-parameter estimates associated to the final C_l-model. This section describes this selection procedure. The performed analyses are based on the results of the MOF-algorithm, validation fit after performing OLS, comparisons with literature, and the visible contributions of regressors to the model output.

Using the MOF selection algorithm, the final model structure for C_n is:

$$\hat{C}_n = C_{n_0} + C_{n_\beta}\beta + C_{n_r}r + C_{n_{\delta_a}}\delta_a + C_{n_{\delta_r}}\delta_r + C_{n_{\Delta X}}\Delta X\frac{y_w}{b} + C_{n_\alpha}\alpha \tag{20}$$

As with the model structure for C_l, stepwise regression consistently rejected the C_{n_p} which effects where captured by the $C_{n_{\Delta X}}\Delta X$ term, leading to potential issues when blending the nominal aerodynamic model with the proposed stall model.

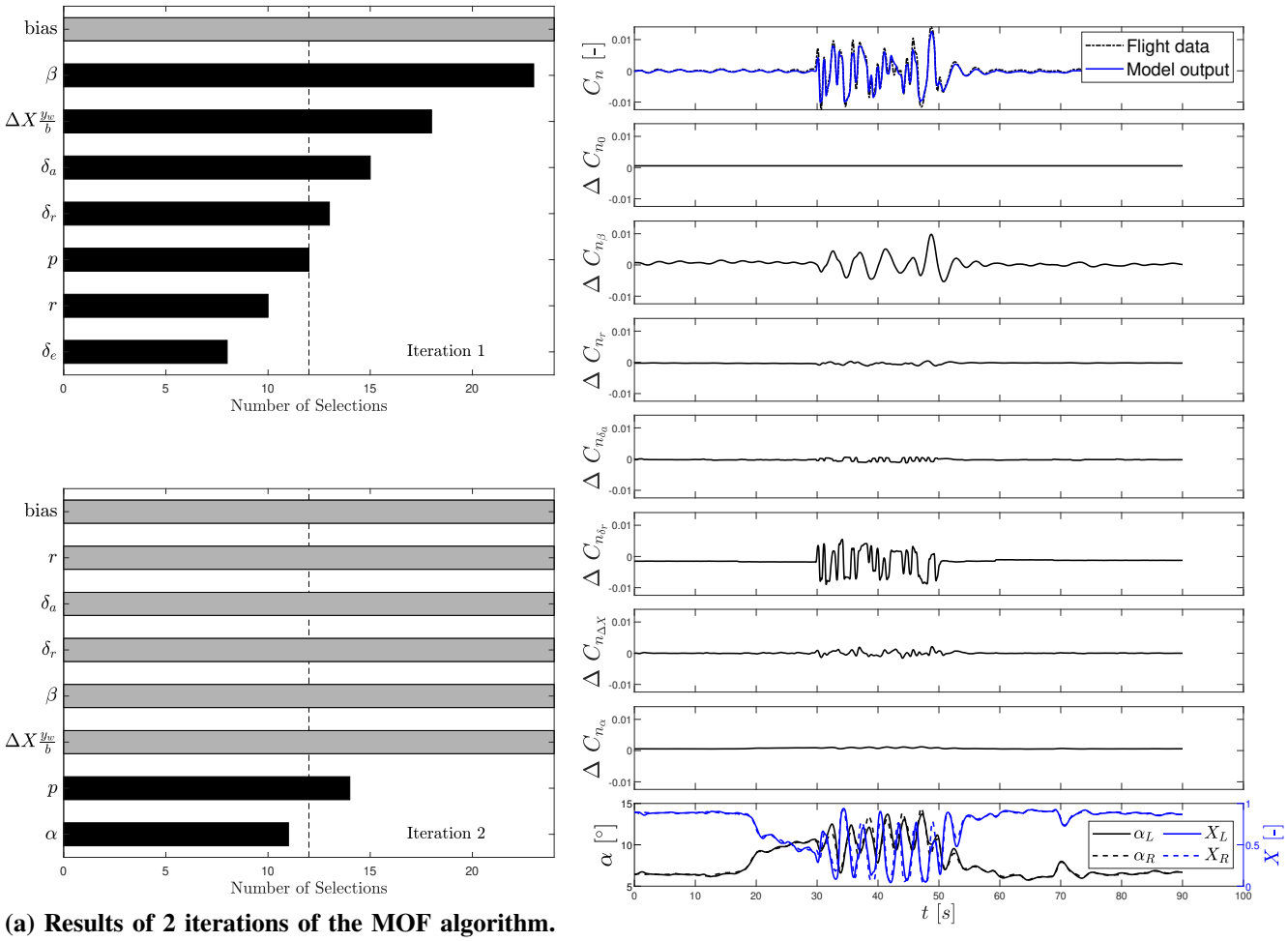

(a) Results of 2 iterations of the MOF algorithm. Grey bars indicate fixed model terms.

(b) Model term contributions, after OLS (ASYM set 16).

Fig. 7 C_n-model structure selection results.

The final model structure for C_Y determined using the MOF selection algorithm is:

$$\hat{C}_Y = C_{Y_0} + C_{Y_\beta}\beta + C_{Y_r}r + C_{Y_{\delta_a}}\delta_a + C_{Y_{\delta_r}}\delta_r + C_{Y_{\Delta X}}\Delta X\frac{y_w}{b} \tag{21}$$

As previously discussed, the longitudinal model structures are taken directly from previous work [15]. For completeness, they are included in this model structure description. The longitudinal model

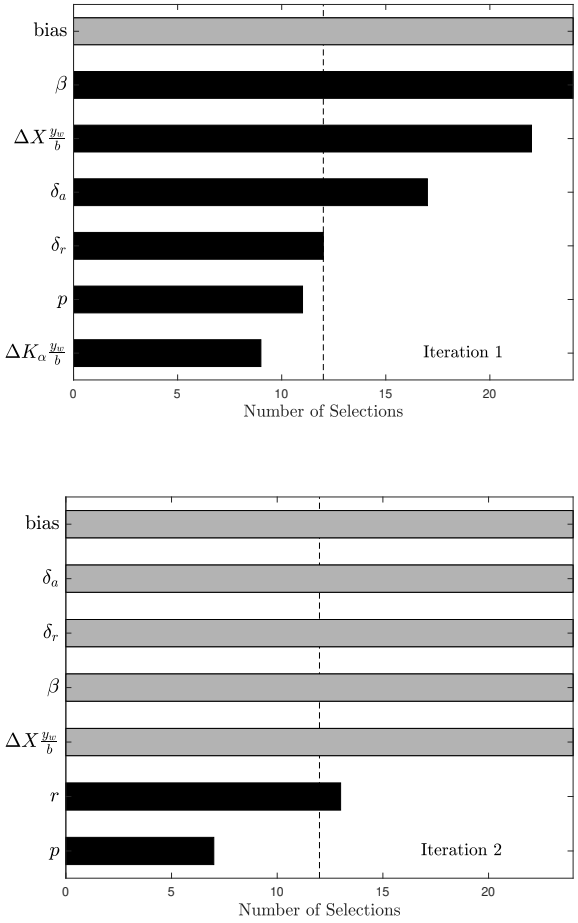

(a) Results of 2 iterations of the MOF algorithm. Grey bars indicate fixed model terms.

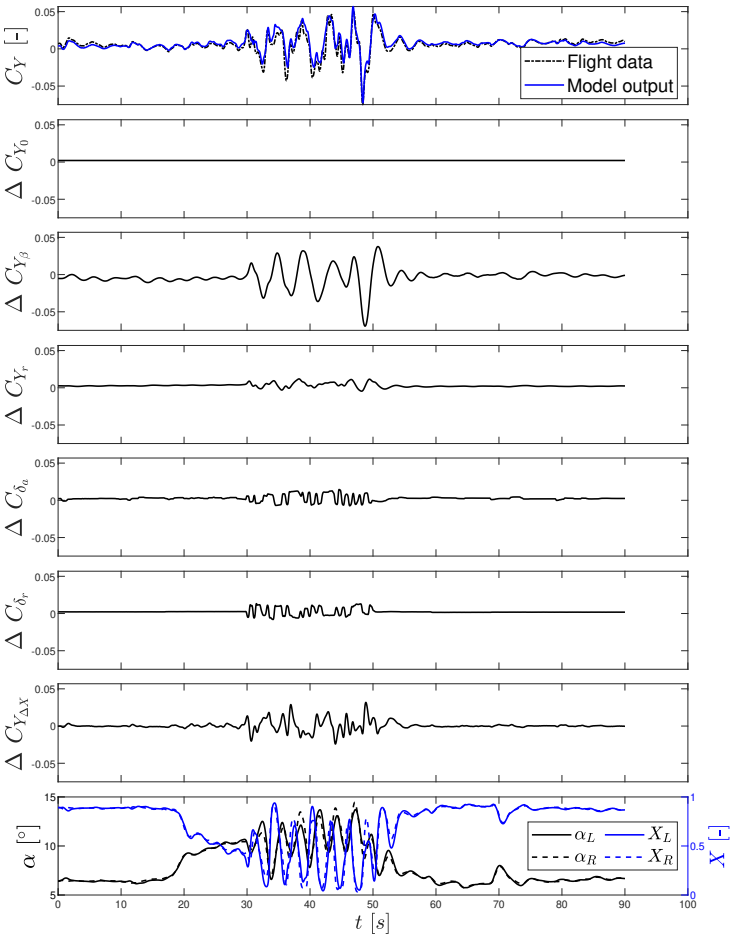

(b) Model term contributions, after OLS (ASYM set 16).

Fig. 8 C_Y-model structure selection results.

structures include three transformations of X, one for each model:

$$\begin{aligned}
\hat{C}_L &= C_{L_0} + C_{L_\alpha}\left(\frac{1+\sqrt{X}}{2}\right)^2 \alpha + C_{L_{\alpha^2}}(\alpha - 6°)_+^2 \\
\hat{C}_D &= C_{D_0} + C_{D_\alpha}\alpha + C_{D_{\delta_e}}\delta_e + C_{D_X}(1-X) + C_{D_{C_T}}C_T \\
\hat{C}_m &= C_{m_0} + C_{m_\alpha}\alpha + C_{m_{X\delta_e}}\max(0.5, X)\delta_e + C_{m_{C_T}}C_T
\end{aligned} \tag{22}$$

The traditional Kirchhoff term is included in the lift model. As Kirchhoff's model was developed for airfoils, a correction term is added to model the entire aircraft lift, based on a univariate spline in α with zero-order continuity:

$$(\alpha - 6°)_+^2 = \begin{cases} (\alpha - 6°)^2 & \text{when} \quad \alpha \geq 6° \\ 0 & \text{when} \quad \alpha < 6° \end{cases} \tag{23}$$

The $(1-X)$-term in the drag model describes a drag increase due to flow separation. Finally, $\max(0.5, X)\delta_e$ in the pitch moment model provides a reducing effect on the elevator effectiveness, with an upper limit of 50% reduction.

4.4 Step IV: Aerodynamic Parameter Estimates

Table 5a and Table 5b present the outcomes of the parameter estimation process for the asymmetric and symmetric aerodynamic model equations, respectively. These tables display the estimated parameter

values, the standard deviations of the estimates across the data sets, and the findings of two statistical tests (one-sample Kolmogorov-Smirnov (KS) test and one-sample t-test).

Table 5 Aerodynamic parameter estimates, with standard deviations and results of statistical tests. KS-test: N = normally distributed, X = not normally distributed. t-test: o = zero-mean, * = not zero-mean,

(a) Asymmetric models.

	Estimates		KS-test		t-test	
θ_{C_i}[-]	$\hat{\theta}$	$\sigma_{\hat{\theta}}$	p	h	p	h
C_{l_0}	-0.0006	0.0004	0.5267	N	0.0389	*
C_{l_β}	-0.0279	0.0108	0.7790	N	0.0000	*
C_{l_r}	0.0661	0.0562	0.8271	N	0.6019	*
$C_{l_{\delta a}}$	-0.0501	0.0104	0.6221	N	0.0000	*
$C_{l_{\Delta X}}$	-0.1274	0.0145	0.7102	N	0.0000	*
C_{n_0}	0.0006	0.0011	0.8810	N	0.0687	o
C_{n_β}	0.0709	0.0093	0.7497	N	0.0000	*
C_{n_r}	-0.0598	0.0590	0.6226	N	0.0000	*
$C_{n_{\delta a}}$	0.0113	0.0043	0.9600	N	0.0000	*
$C_{n_{\delta r}}$	0.0493	0.0267	0.1090	N	0.0000	*
$C_{l_{\Delta X}}$	-0.0302	0.0110	0.3024	N	0.0000	*
C_{n_α}	0.0049	0.0056	0.5810	N	0.0000	*
C_{Y_0}	0.0021	0.0100	0.5576	N	0.2691	o
C_{Y_β}	-0.5013	0.0629	0.9420	N	0.0000	*
C_{Y_r}	0.6204	0.5314	0.8824	N	0.0001	*
$C_{Y_{\delta a}}$	-0.1344	0.0390	0.9847	N	0.0000	*
$C_{Y_{\delta r}}$	-0.0725	0.2683	0.2270	N	0.0917	o
$C_{Y_{\Delta X}}$	-0.4588	0.0663	0.8865	N	0.0000	*

(b) Symmetric models.

	Estimates		KS-test		t-test	
θ_{C_i}[-]	$\hat{\theta}$	$\sigma_{\hat{\theta}}$	p	h	p	h
C_{L_0}	0.2480	0.0897	0.9210	N	0.0000	*
C_{L_α}	4.3991	0.8553	0.7341	N	0.0000	*
$C_{L_{\alpha^2}}$	18.854	5.2721	0.3663	N	0.0000	*
C_{D_0}	-0.0078	0.0167	0.9037	N	0.0038	o
C_{D_α}	0.3372	0.1219	0.7914	N	0.0000	*
$C_{D_{\delta_e}}$	-0.1715	0.0743	0.8754	N	0.0000	*
$C_{D_{1-X}}$	0.0246	0.0120	0.9937	N	0.0000	*
$C_{D_{C_T}}$	0.4301	0.0743	0.6382	N	0.0000	*
C_{m_0}	0.0324	0.0190	0.9607	N	0.0000	*
C_{m_α}	-0.5497	0.1171	0.6830	N	0.0000	*
$C_{m_{\delta_e X}}$	-0.9220	0.1445	0.8446	N	0.0000	*
$C_{m_{C_T}}$	0.0857	0.0974	0.9830	N	0.0004	*

4.5 Stall Model Validation

The presented aerodynamic parameters have resulted in a 6-DOF stall model that should be capable of adequately describing the nonlinearities of flow separation. To validate the model, the model fit is evaluated using the validation data set. This data set contains 6 stall maneuvers and was not used in the identification phase.

The validation fit is visualized in Fig. 9, which presents the model output of the best- and worst-performing validation sets. Both Table 6 and Fig. 9 present a satisfactory agreement with the data of the lateral-directional models. This result confirms that using a flow separation differential in the roll moment model structure allows for the identification of asymmetric flow separation characteristics. Moreover, the identified flow separation variables are capable of adequately capturing the nonlinearities of the lateral force and the yaw moment.

Conversely, the longitudinal models present a lacking description of the flight data, most notably because of the lack of pitch damping provided by the model, which is caused by averaging of the (highly) dynamic pitch damping over the complete stall maneuver. The model structures were directly taken from a validated stall model [15]. X is computed by averaging the local flow separation variables X_L and X_R, which are each evaluated using the roll-based X-parameter estimates. This approach is less suitable for

longitudinal stall modeling using Kirchhoff's method, as the resulting flow separation variable is not fully capable of accurately describing the flow separation effects of the drag and the pitch moment.

Table 6 Aerodynamic model fit properties, averaged over the training sets and validation sets.

	Training				Validation			
Model	MSE	$\bar{R^2}$	$min(R^2)$	$max(R^2)$	MSE	$\bar{R^2}$	$min(R^2)$	$max(R^2)$
C_l	1.03E-6	0.77	0.42	0.89	1.41E-6	0.75	0.63	0.86
C_n	4.85E-7	0.65	0.27	0.89	8.50E-7	0.68	0.36	0.92
C_Y	4.11E-5	0.63	0.16	0.92	5.73E-5	0.65	0.25	0.89
C_L	4.09E-3	0.80	0.55	0.91	3.51E-3	0.78	0.67	0.87
C_D	1.13E-4	0.70	-0.15	0.84	1.10E-4	0.67	0.29	0.80
C_m	2.10E-4	0.50	-0.34	0.80	1.83E-4	0.43	-0.25	0.64

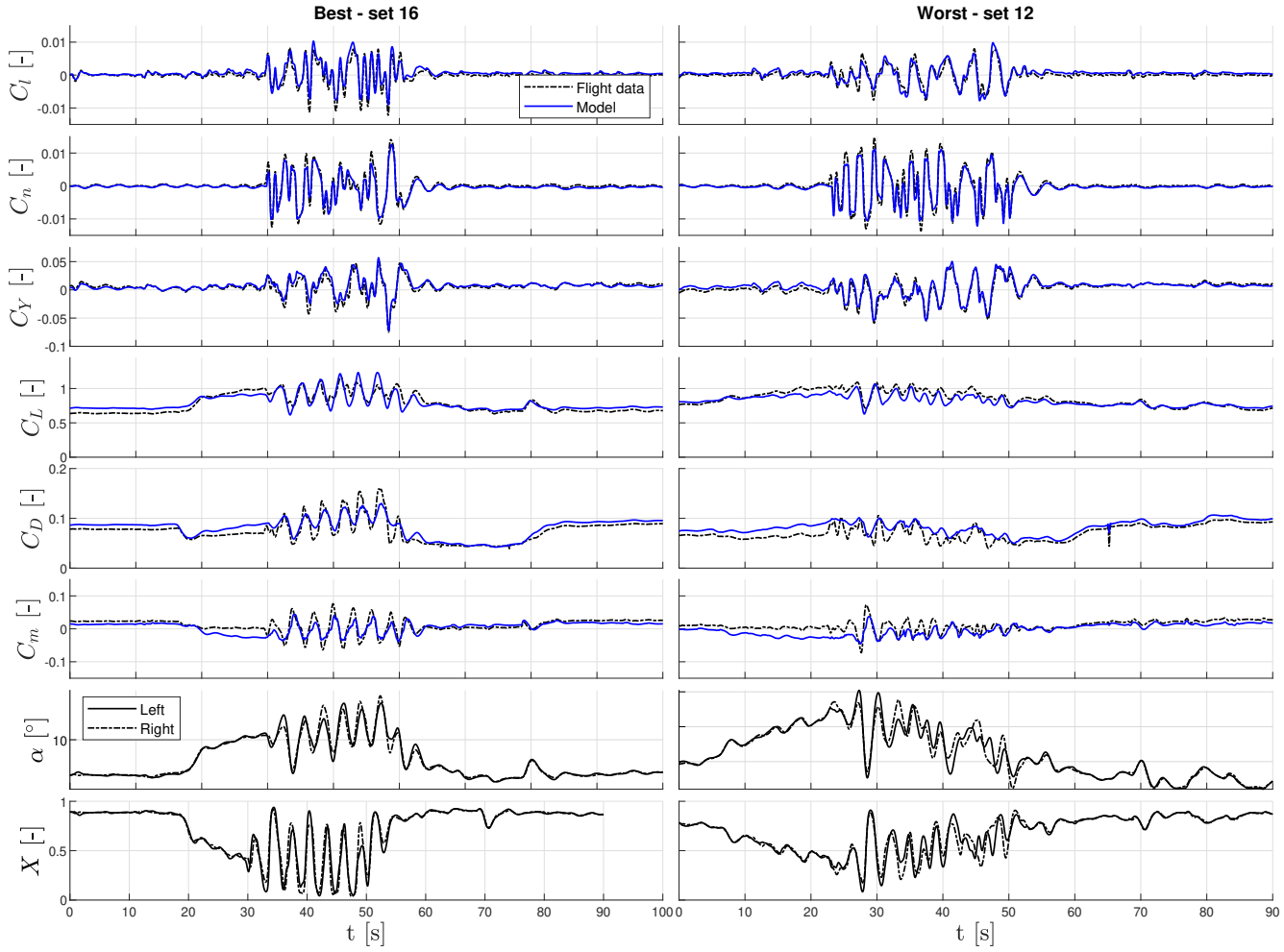

Fig. 9 Model validation plots, presenting the model output of the best- and worst-performing validation sets.

5 Discussion

This research has presented a methodology for identifying asymmetry in aircraft stall characteristics, based on flight data acquired using a Cessna Citation II laboratory aircraft. This section discusses the results of the presented model, by comparing them with previous models of the aircraft. Several aerodynamic models have been developed for this Cessna Citation II aircraft. A numerical performance comparison can be found in Table 7, which presents the validation fit metrics for the proposed model, the baseline stall model [15], and the nominal envelope model [22]. The last-mentioned model does not include specific stall-related dynamics and was identified in the normal flight envelope. It is included in this comparison to evaluate the merit of the current methodologies. The longitudinal model structures of the proposed model and the baseline stall model are equal but feature different X-parameter values, and therefore different aerodynamic parameter estimates. The observations are visualized for an example maneuver in Figs. 10a and 10b, for the lateral-directional the longitudinal axes, respectively.

The proposed model showcases the best prediction performance for C_l, C_n, and C_Y. In comparison to the lateral-directional outputs of the baseline stall model on the ASYM data set, the MSE reduces with 56%, 52%, and 35% respectively. Refer to Table 7 for all relative differences in MSE and R^2 with respect to the baseline model. The proposed methodology of estimating flow separation parameters from the roll moment has proven effective at improving the lateral-directional model fidelity. Conversely, the fidelity of the longitudinal models C_L, C_D, and C_m worsens with the new X-parameters, as the previous model performs greater in terms of MSE and R^2. Moreover, the proposed model performs better than the nominal envelope model, in every axis.

In order to take advantage of both methodologies, a hybrid approach can be applied. In this case, two X-parameter sets can be defined: $(\theta_X)_s$ and $(\theta_X)_a$. The symmetric flow separation variable X is computed using $(\theta_X)_s$ and the angle of attack at the C.G., while the asymmetric flow separation variables X_L, X_R are computed using $(\theta_X)_a$ and the local angles of attack. This approach would require no additional optimizations, as the models were identified for similar flight conditions, and the lift-based model has shown a good fit on the current validation data set. TUsing the hybrid approach with $(\theta_X)_s = [0.2547, 0.0176, 27.671, 0.2084]^\top$ [15] and $(\theta_X)_a = [0.0971, 0.5526, 16.865, 0.1730]^\top$ (the estimates of this paper) results in the lateral-directional model fit properties in the first column of Table 7 and the longitudinal properties of the second column. It should be noted that with such a hybrid approach, the flow separation variables lose their physical meaning since $(\theta_X)_s$ and $(\theta_X)_a$ may no longer be correlated.

Table 7 Comparison of the proposed model performance with previous Cessna Citation II models. The model fit properties are computed for the 6 validation sets, including the relative difference with respect to the baseline model.

	Proposed Stall Model		**Baseline Stall Model** [15]		**Nominal Envelope Model** [22]	
Model	MSE	$\bar{R}^2$	MSE	$\bar{R}^2$	MSE	$\bar{R}^2$
C_l	1.41E-6 (-56%)	0.75 (+70%)	3.20E-6	0.44	5.21E-5 (+1530%)	-6.24
C_n	8.50E-7 (-52%)	0.68 (+196%)	1.80E-6	0.23	5.39E-5 (+2890%)	-18.9
C_Y	5.73E-5 (-35%)	0.65 (+30%)	8.86E-5	0.50	3.57E-3 (+3930%)	-15.2
C_L	3.51E-3 (+142%)	0.78 (-14%)	1.45E-3	0.91	5.37E-3 (+270%)	0.64
C_D	1.10E-4 (+90%)	0.67 (-20%)	5.78E-5	0.84	1.94E-3 (+3250%)	-5.02
C_m	1.83E-4 (+31%)	0.43 (-31%)	1.39E-4	0.62	1.22E-3 (+780%)	-2.84

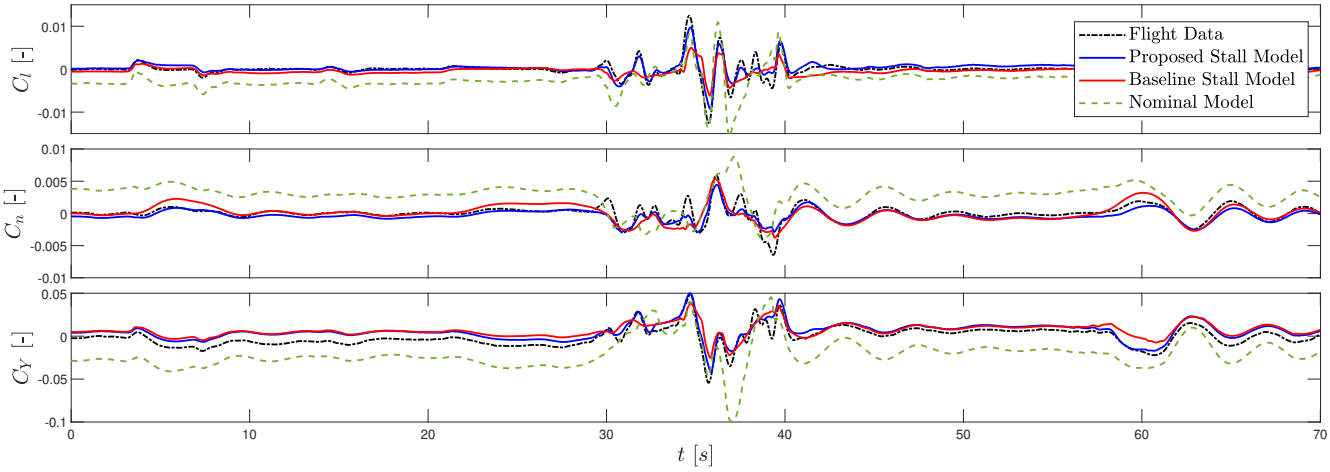

(a) Asymmetric models.

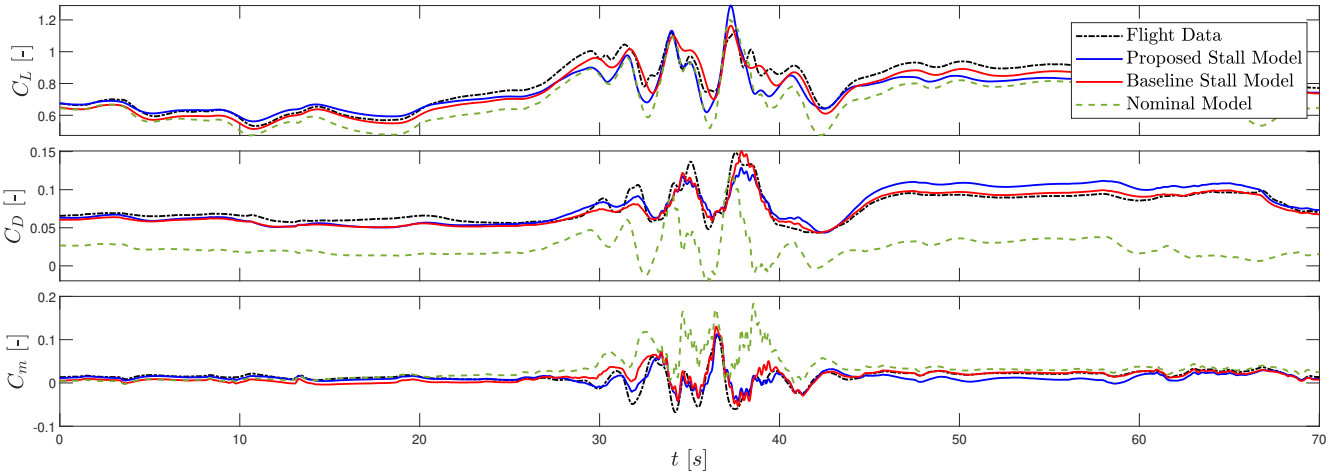

(b) Symmetric models.

Fig. 10 A comparison of the flight data, the proposed stall model output, the baseline stall model [15], and the nominal envelope model [22].

6 Conclusion

This research set out to improve the lateral-directional model fidelity of the existing Cessna Citation II dynamic stall model. For this purpose, a flight test data set of stall maneuvers was specifically collected to induce asymmetric flow separation effects. The accelerated stall maneuvers included dynamic inputs in two axes, and a subset of maneuvers was approached with a reference sideslip angle. Kirchhoff's stall modeling method was modified to include two distinct flow separation variables, each describing the separation development on the respective wing surface. The parameters describing these variables were estimated using the roll moment derived from flight data, which is a novel approach. The lateral-directional model outputs provide a good fit with the validation flight data set, with an average explained variance of 0.70, and an average improvement of 48% in terms of MSE, compared to the baseline stall model. Our results indicate that the estimated flow separation parameters are less suitable for longitudinal stall modeling than for lateral-directional stall modeling. Acknowledging this fact, a hybrid Kirchhoff method is proposed, which combines two sets of parameters describing symmetric and asymmetric flow separation separately.

References

[1] G.H. Bryan. *Stability in Aviation: an Introduction to Dynamical Stability as Applied to the Motion of Aeroplanes*. Macmillan and Company, London, 1911.

[2] M. Fouda and H.E. Taha. Effect of Wing Planform on Airplane Stability and Control Authority in Stall. *AIAA Science and Technology Forum and Exposition, AIAA SciTech Forum 2022 San DIego, CA, USA*, 2022. DOI: 10.2514/6.2022-1161.

[3] D.H. Nguyen, M.G. Goman, M.H. Lowenberg, and S.A. Neild. Evaluating Unsteady Aerodynamic Effects in Stall Region for a T-Tail Transport Model. In *AIAA Science and Technology Forum and Exposition, AIAA SciTech Forum 2022*. American Institute of Aeronautics and Astronautics Inc, AIAA, 2022. ISBN: 9781624106316. DOI: 10.2514/6.2022-1932.

[4] N.B. Abramov, M.G. Goman, A.N. Khrabrov, and B.I. Soemarwoto. Aerodynamic modeling for poststall flight simulation of a transport airplane. In *Journal of Aircraft*, volume 56, pages 1427–1440. American Institute of Aeronautics and Astronautics Inc., 2019. DOI: 10.2514/1.C034790.

[5] A. A. Lambregts, G. Nesemeier, J. E. Wilborn, and R. L. Newman. Airplane upsets: Old problem, new issues. In *AIAA Modeling and Simulation Technologies Conference and Exhibit Honolulu, Hawaii, USA*, number August, pages 1115–1125, 2008. ISBN: 9781563479458. DOI: 10.2514/6.2008-6867.

[6] A. Da Ronch, D. Vallespin, M. Ghoreyshi, and K. J. Badcock. Evaluation of dynamic derivatives using computational fluid dynamics. *AIAA Journal*, 50(2):470–484, 2 2012. ISSN: 00011452. DOI: 10.2514/1.J051304.

[7] M.H. Smaili, B.I. Soemarwoto, N.B. Abramov, M.G. Goman, A.N. Khrabrov, E.N. Kolesnikov, and L. Fucke. Pushing Ahead-SUPRA Airplane Model for Upset Recovery. Technical report, 2017. `www.nlr.nl`.

[8] M. Goman and A. Khrabrov. State-space representation of aerodynamic characteristics of an aircraft at high angles of attack. In *Astrodynamics Conference Hilton Head Island, SC, USA*, pages 759–766. American Institute of Aeronautics and Astronautics Inc, AIAA, 1992. DOI: 10.2514/6.1992-4651, `https://arc.aiaa.org/doi/10.2514/6.1992-4651`.

[9] D. Fischenberg. Identification of an unsteady aerodynamic stall model from flight test data. In *20th Atmospheric Flight Mechanics Conference Baltimore, MD, USA*, pages 138–146. American Institute of Aeronautics and Astronautics Inc, AIAA, 1995. ISBN: 9780000000002. DOI: 10.2514/6.1995-3438, `https://arc.aiaa.org/doi/10.2514/6.1995-3438`.

[10] J.N. Dias. Unsteady and Post-Stall Model Identification Using Dynamic Stall Maneuvers. In *AIAA Atmospheric Flight Mechanics Conference Dallax, TX, USA*. American Institute of Aeronautics and Astronautics (AIAA), 6 2015. DOI: 10.2514/6.2015-2705.

[11] D. Fischenberg and R.V. Jategaonkar. Identification of Aircraft Stall Behavior from Flight Test Data. In *RTO SCI Symposium on System Identification for Integrated Aircraft Development and Flight Testing Madrid, Spain*, 1998. DOI: https://doi.org/10.2514/6.1996-3441, `https://arc.aiaa.org/doi/abs/10.2514/6.1996-3441`.

[12] J. Singh and R. V. Jategaonkar. Flight determination of configurational effects on aircraft stall behavior. In *21st Atmospheric Flight Mechanics Conference San Diego, CA, USA*, volume 33, pages 657–665. American Institute of Aeronautics and Astronautics, 5 1996. DOI: 10.2514/6.1996-3441, `http://arc.aiaa.org`.

[13] F.H. Lutze, Y. Fan, and G. Stagg. Multiaxis unsteady aerodynamic characteristics of an aircraft. In *24th Atmospheric Flight Mechanics Conference*, pages 56–64. American Institute of Aeronautics and Astronautics Inc, AIAA, 1999. DOI: 10.2514/6.1999-4011.

[14] Christoph Deiler. Aerodynamic modeling, system identification, and analysis of iced aircraft configurations. *Journal of Aircraft*, 55(1):145–161, 2018. DOI: 10.2514/1.C034390.

[15] J.B. van Ingen, C.C. de Visser, and D.M. Pool. Stall model identification of a cessna citation II from flight test data using orthogonal model structure selection. *AIAA Scitech 2021 Forum Virtual Event*, pages 1–29, 2021. DOI: 10.2514/6.2021-1725.

[16] E.A. Morelli, K. Cunningham, and M.A. Hill. Global Aerodynamic Modeling for Stall/Upset Recovery Training Using Efficient Piloted Flight Test Techniques. In *AIAA Modeling and Simulation Technologies (MST) Conference Boston, MA, USA*, 2013. DOI: https://doi.org/10.2514/6.2013-4976, `https://arc.aiaa.org/doi/10.2514/6.2013-4976`.

[17] M. Mulder, B. Lubbers, P.M.T. Zaal, M.M. Van Paassen, and J.A. Mulder. Aerodynamic Hinge Moment Coefficient Estimation Using Automatic Fly-By-Wire Control Inputs. In *AIAA Modeling and Simulation Technologies Conference - Chicago, Illinois*, 2009.

[18] J.A. Grauer. Position Corrections for Airspeed and Flow Angle Measurements on Fixed-Wing Aircraft. *NASA TM*, 219795, 2017.

[19] V Klein and E Morelli. *Aircraft System Identification: Theory and Practice*. AIAA, 2006.

[20] E.A. Morelli. Global nonlinear aerodynamic modeling using multivariate orthogonal functions. *Journal of Aircraft*, 32(2):270–277, 5 1995. ISSN: 00218669. DOI: 10.2514/3.46712.

[21] V. Klein, Batterson J.G., and P.C. Murphy. Determination of Airplane Model Structure from Flight Data by Using Modified Stepwise Regression. *NASA Technical Paper*, 1916, 10 1981.

[22] M.A. Van Den Hoek, C.C. De Visser, and D.M. Pool. Identification of a Cessna Citation II Model Based on Flight Test Data. In *4th CEAS Specialist Conference on Guidance, Navigation & Control*, 2017.